Frequency Down-Conversion of Dual-Wavelength Raman Fiber Laser in PPLN-Based Optical Parametric Oscillator
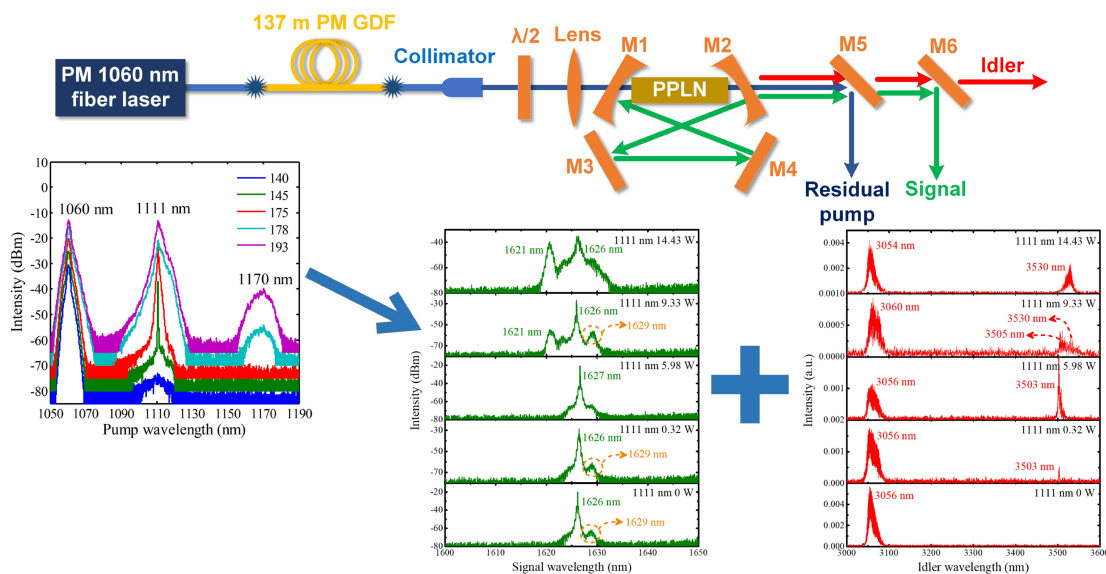
Peng Wang
Xi Cheng
Xiao Li
Xiaojun Xu
Kai Han
Jian Chen

Frequency Down-Conversion of Dual-Wavelength Raman Fiber Laser in PPLN-Based Optical Parametric Oscillator

Peng Wang [ORCID],[1] **Xi Cheng** [ORCID],[1] **Xiao Li** [ORCID],[1] **Xiaojun Xu**,[1] **Kai Han**,[1] **and Jian Chen**[2]

[1]College of Advanced Interdisciplinary Studies, National University of Defense Technology, Changsha 410073, China
[2]Anhui Province Key Laboratory of Non-Destructive Evaluation, ZC Optoelectronic Technologies, Ltd., Hefei 230000, China

Abstract: We report on frequency down-conversion of dual-wavelength (DW) Raman fiber laser in a periodically poled lithium niobate-based optical parametric oscillator. The DW pump source was fixed at 1060 and 1111 nm that was obtained based on stimulated Raman scattering effect by combining a home-made linearly polarized 1060-nm fiber laser and 137-m-long polarization-maintaining passive fiber. The total pump power went through three stages, in the latter two of which the 1111-nm wave appeared. In the entire experiment, the 1060-nm pump beam achieved parametric oscillation and generated 1626-nm signal beam and 3056-nm idler beam. The 1111-nm pump beam generated 3503-nm idler beam based on difference frequency generation (DFG) between itself and 1626-nm signal beam in the second stage. With power enhancement, it built independent parametric oscillation in the third stage and generated 1621-nm signal beam as well as 3530-nm idler beam. The DW idler power ranged from 3.94 to 7.78 W in the latter two stages. The power and efficiency characteristics in frequency conversion processes of 1060- and 1111-nm pump beams were also analyzed separately.

Index Terms: Infrared lasers, fiber lasers, nonlinear crystals, nonlinear.

1. Introduction

DW mid-infrared sources around $3 \sim 5$ μm are of great application in many fields such as chemical sensing, terahertz-wave (THz-wave) generation and differential absorption lidars [1]–[3]. OPOs are now well-established mid-infrared sources offering coherent light, high power, broad bandwidth and wide tuning range, and have been widely investigated [4]–[8]. Compared with other kinds of pump sources, fiber lasers have many advantages such as high efficiency, excellent beam quality, compact structure and good portability [9], [10]. Benefitting from these, fiber-laser-pumped DW mid-infrared OPOs have been demonstrated for a long time. Adopting two nonlinear crystals in a resonant cavity is an effective way to obtain DW mid-infrared output. In 2015, Yuwei Jin et al demonstrated a fiber-laser-pumped two-crystal mid-infrared OPO. The singly-resonant cavity containing two MgO:periodically poled lithium niobate (PPLN) crystals was capable of
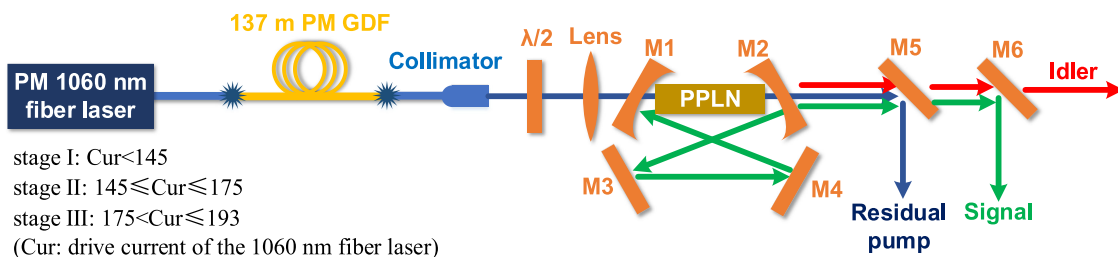
Fig. 1. Schematic diagram of DW-Raman-fiber-laser-pumped OPO.

obtaining two idler wavelengths, independently tunable over 30 THz in the 2.9 $\sim$ 4.2 μm region [11]. V. Ramaiah-Badarla used the similar setup, in which two independent OPO processes occurred and obtained DW idler output tunable across 3118–3393 nm [12]. Another method for DW mid-infrared generation is making use of nonlinear crystals with special poled structure. Peipei Jiang et al reported a fiber-laser-pumped DW mid-infrared OPO based on an aperiodically poled MgO:LN (APPLN) wafer. Using a linearly polarized Yb fiber laser at 1064 nm, mid-infrared emissions at 3.3 and 3.8 μm were obtained simultaneously from the OPO [13]. Shuangshuang Cai demonstrated a gain-switched fiber laser pumped DW OPO operating around 3–5 μm, in which the nonlinear crystal was also a bulk of APPLN [14]. In addition to above methods, employing DW fiber lasers as pump sources was also an effective way for DW mid-infrared generation. Recently, our research group reported DW mid-infrared OPO based on synchronous parametric oscillation and intracavity DFG, pumped by DW fiber lasers that were achieved by combining two lasers in series [15].

The SRS effect is a common fiber nonlinear effect and has been deeply researched [16]–[19]. DW fiber lasers based on SRS effect have been demonstrated [20]–[23] and can be used as the pump source of DW mid-infrared OPO for the time being. In this paper, we demonstrated a DW mid-infrared OPO, pumped by a DW Raman fiber laser fixed at 1060 nm and 1111 nm. Along with enhancement of SRS effect, the total, 1060 nm and 1111 nm pump power went through three stages. The 1111 nm pump beam arose in the latter two stages. In the second stage, one signal and two idler beams were obtained which were located at 1626 nm, 3056 nm and 3503 nm. It was analyzed that the 1060 nm pump beam built parametric oscillation and the 1111 nm pump beam participated in DFG process between itself and 1626 nm signal beam. In the final stage, two pairs of signal and idler beams were obtained at 1621 nm and 3530 nm, 1626 nm and 3056 nm separately. Both two pump beams reached threshold and built two independent OPO processes. The DW idler power in the latter two stages ranged from 3.94 W to 7.78 W, in which the 3.1 μm and 3.5 μm idler power had no fixed relationship and fluctuated with the corresponding pump power. This is, to the best of our knowledge, the first report on a DW mid-infrared OPO pumped by a DW Raman fiber laser. It was also the first time to combine fiber nonlinear effect and crystal nonlinear effect for frequency conversion. Compared with other methods, its structure was very simple and easy to construct. The obtained 3056 nm mid-infrared radiation is applicable for medical and biologic applications [24]–[26], and as pump source for generating long-wavelength infrared radiation [27] while the 3503/3530 nm mid-infrared radiation can be used for trace gas sensing [28]–[30]. Besides, the DW mid-infrared radiation can also be used for synchronous detection of multicomponent gas [28]. The experiment results also revealed great potential in multi-wavelength mid-infrared generation with large wavelength gap using higher-order SRS effect.

2. Experiment Setup

The schematic diagram of the DW mid-infrared OPO is depicted in Fig. 1. The pump source was a home-made linearly polarized 1060 nm fiber laser with the maximum output power of 71.1 W. It was fused with 137 m PM 10/125 μm passive fiber which was bought from Nufern Corporation. A fiber collimator was used to enable the pump beam parallel and a half-wave plate (HWP) was
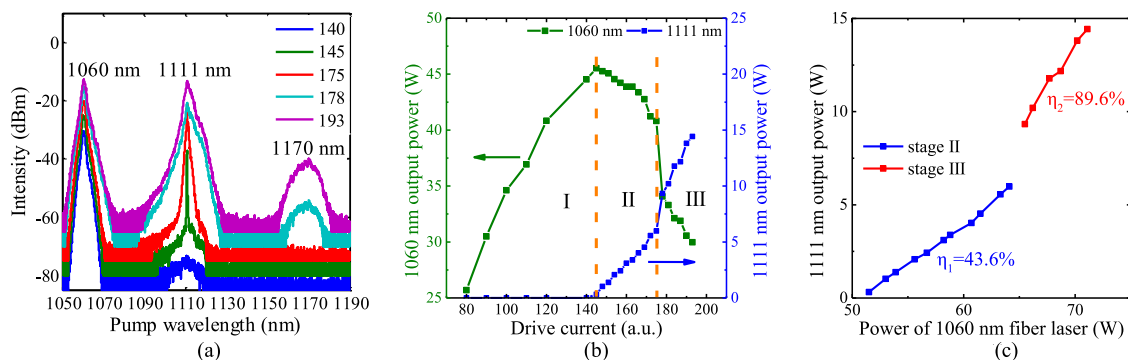
Fig. 2. (a) Measured spectra of DW pump beam under different drive current. (b) Measured 1060 nm and 1111 nm output power versus drive current. (c) Measured 1111 nm output power versus power of 1060 nm fiber laser.

placed behind the collimator to align the polarization direction of pump beam accordingly. After the HWP is a focusing lens which focused the pump beam into the center of PPLN crystal. The radius of beam waist was measured to be about 80 μm. The OPO resonant cavity was designed as a typical four-mirror ring cavity which was composed of two concave mirrors M1 and M2 with the curvature radius of 150 mm, two plane mirrors M3 and M4. Three mirrors, M1, M3 and M4, were antireflection (AR) coated of high transmission (T > 95%) over 1–1.1 μm and 3–4 μm for the pump and idler, and high reflectivity (R > 99%) over 1.4–1.7 μm for the signal, ensuring singly resonant oscillation (SRO). The output coupling mirror, M2, was high transmissive for the pump and idler, and partially transmissive (T ∼ 10%, non-optimized) for the signal. The nonlinear crystal is a 50-mm-long MgO:PPLN with an aperture of 10 mm*1 mm. It was periodically poled with a grating period of Λ = 31.12 μm. Both two end faces were carefully grounded and polished, and AR-coated of high transmission for the pump, signal and idler beams. Two dichroic mirrors, M5 and M6, were used to separate the residual pump, signal and idler beams.

3. Experiment Results and Discussion

By blocking the light path inside the cavity, the pump beam was able to pass through the whole cavity with no frequency conversion. The DW pump spectra under different drive current of 1060 nm fiber laser were measured and shown in Fig. 2(a). The figure indicates that obvious SRS effect appeared when the drive current reached 145. The Raman radiation was centered at 1111 nm and the frequency shift was calculated to be 13.48 THz. The output pump beam always had two central wavelengths located at 1060 nm and 1111 nm when the drive current increased from 145 to 175. The intensity difference between 1060 nm and 1111 nm beams was about 12 dB at the beginning and decreased to 1.5 dB at the drive current of 175. The second-order SRS effect appeared when the drive current reached 178 and the newly generated Raman radiation was located at 1170 nm. No higher-order SRS effect was observed when the drive current reached the maximum of 193. The intensity difference between 1111 nm and 1170 Raman laser was 35 dB at the drive current of 178 and finally decreased to 27 dB. The 1111 nm linewidth was much smaller than the 1060 nm linewidth when the drive current was between 145 to 175 and suddenly got broadened, much larger than the 1060 nm radiation when the drive current reached 178. The 1170 nm linewidth was even larger than the 1111 nm radiation. The outputted 1060 nm and Raman beams were separated using a dichroic mirror, and their power versus drive current was measured and drawn in Fig. 2(b). The measured Raman laser power was totally regarded as 1111 nm laser power because it was at least 500 times larger than the 1170 nm laser power. As can been seen from the figure that the 1060 nm and 1111 nm laser power went through three stages as shown by two brown dotted lines. In stage I when the drive current didn't reach 145, no 1111 nm radiation appeared and the 1060 nm power linearly increased to 44.53 W. In stage II when the drive current ranged from 145 to 175, the
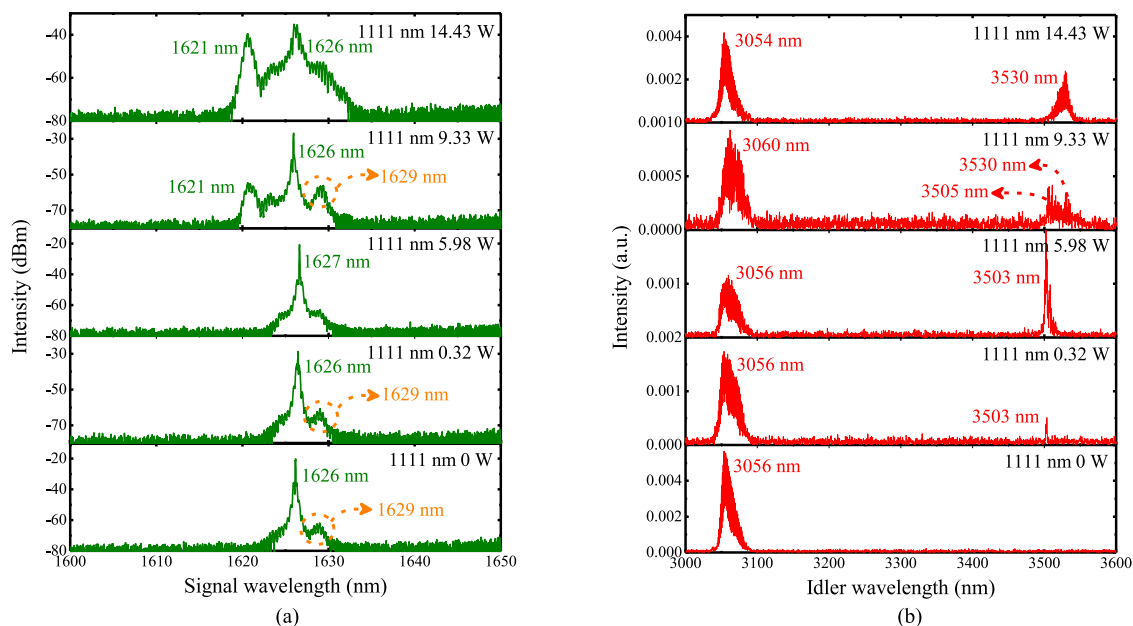
Fig. 3. Measured (a) signal and (b) idler spectra under different 1111 nm pump power.

1111 nm laser appeared, and its power linearly increased from 0.32 W to 5.98 W while the 1060 nm laser power decreased from 45.52 W to 40.81 W. In stage III when the drive current reached 178 and became higher, the 1111 nm laser power firstly jumped to 9.33 W and then linearly increased to 14.43 W while the 1060 nm laser power dropped to 34.1 W and then gradually decreased to 30 W. It is obvious that the abrupt power change arose together with spectrum broadening of 1111 nm Raman laser and appearance of second-order SRS effect. Figure 2(c) reveals the relationship between the 1111 nm laser power and 1060 nm fiber laser power. It indicated that the threshold of first and second order SRS effect was 51.5 W and 65.5 W separately. The pump-to-Raman slope efficiency in stage II and III was calculated to be 43.6% and 89.6% relatively. It was analyzed that the resonant cavity used in the experiment was an integrated module whose photo was shown in Ref. [31] and no optical isolator was adopted to prevent back-reflection laser caused by residual reflection of cavity mirrors. The back-reflection laser became high enough when the power of 1060 nm fiber laser reached 65.5 W. Part of it was coupled again into the fiber and greatly enhanced the SRS effect, resulting in appearance of second-order SRS effect and sudden increase of Raman laser power.

The signal and idler spectra under different 1111 nm pump power were measured using an optical spectrum analyzer and a wavemeter, and shown in Fig. 3. As can be seen that the signal and idler beams were fixed at 1626 nm and 3056 nm separately before the SRS effect arose. When the 1111 nm pump power was between 0.32 W to 5.98 W, there still existed just one signal beam centered at 1626 nm, but two idler beams were detected with central wavelengths of 3056 nm and 3503 nm. It indicates that the 1060 nm and 1111 nm pump beams shared the same signal beam and generated two idler beams in stage II. Obviously, the 1626 nm signal beam and 3056 nm idler beam was still generated by the 1060 nm pump beam. However, the 3503 nm idler beam was induced by phase-mismatched DFG process between 1111 nm pump beam and 1626 nm signal beam. The relationship between their wavelengths also fitted with the energy conservation law. When the 1111 nm pump power reached 9.33 W and became higher, a new signal beam centered at 1621 nm appeared. The intensity difference between 1621 nm and 1626 nm signal beams was about 28 dB at the beginning and finally decreased to 4.5 dB. It was analyzed that in stage III, the 1111 nm pump beam reached the threshold and built independent oscillation, resulting in the generation of 1621 nm signal beam. When the 1111 nm pump power was 9.33 W, one idler beam
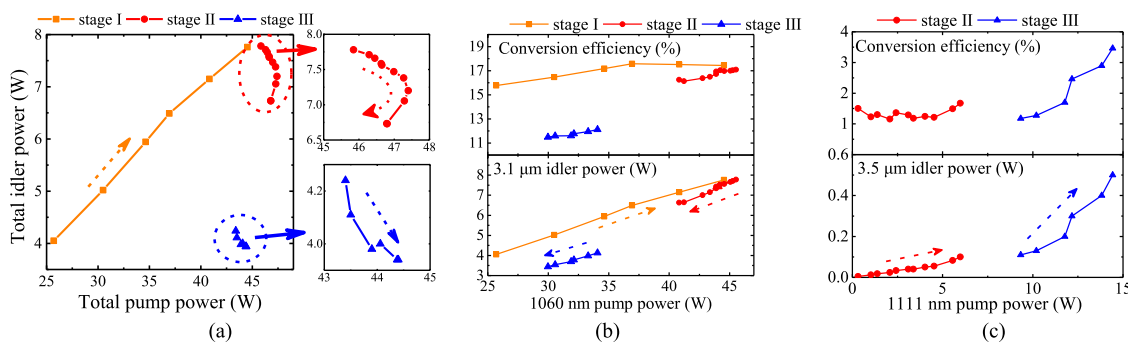
Fig. 4. (a) Total idler power versus total pump power. (b) 3.1 μm idler power and conversion efficiency versus 1060 nm pump power. (c) 3.5 μm idler power and conversion efficiency versus 1111 nm pump power.

was still fixed at 3060 nm, but the longer-wavelength idler beam became wide and anomalous. Two peaks existing in the spectrum were about 3505 nm and 3530 nm. It indicated that the 3505 nm DFG idler beam was still achieved while the 3530 nm idler beam was generated based on parametric oscillation of 1111 nm pump beam. It was analyzed that at this power level, the parametric gain of OPO was almost the same as that of DFG for the 1111 nm pump beam. When the 1111 nm pump beam reached the maximum of 14.43 W, the 3505 nm idler beam disappeared and just 3530 nm and 3054 nm idler beams were detected. It reveals that at this power level, the parametric gain of OPO became much higher than that of DFG for the 1111 nm pump beam, resulting in disappearance of DFG process. Another fact shown in Fig. 3(a) was that no matter how large the 1111 nm pump power was, a broad peak always appeared in the signal spectra, which was fixed at 1629 nm and 30 $\sim$ 40 dB lower than the 1626 nm signal beam. It was caused by the manufacturing imperfection of PPLN crystal and generated by the 1060 nm pump beam. However, it was so weak and the corresponding idler power was surely low, which gave the reason for its absence in the idler spectra. In the further research, better crystal would be adopted for more precise and perfect results.

The relationship between total idler power and total pump power was drawn in Fig. 4(a). The corresponding parts of stage II and III were enlarged and shown in two attached figures on the right of the main figure. The dotted arrows represented variation trend of total pump power. The 3056 nm and 3503/3530 nm idler beams were written for short as 3.1 μm and 3.5 μm idler beams. As can be seen from the figure that in stage I without SRS effect, just 3.1 μm idler beam existed and its power linearly increased from 4.05 W to 7.76 W when the 1060 nm pump power ranged from 25.7 W to 44.5 W. In stage II, the DW idler power decreased from 7.78 W to 6.73 W when the total pump power change from 45.8 W to 47.4 W and then to 46.8 W. In stage III, the DW idler power exhibited a sudden drop from 6.73 W to 4.24 W, similar to the total pump power and finally decreased to 3.94 W. The 3.1 μm and 3.5 μm idler beams were separated using a dichroic mirror and their power as well as conversion efficiency versus each pump power was shown in Fig. 4(b) and (c). The dotted arrows represented variation trend of 1060 nm and 1111 nm pump power. With change of 1060 nm pump power, the 3.1 μm idler power linearly increased from 4.05 W to 7.76 W in stage I, declined to 6.63 W in stage II, dropped to 4.13 W and finally decreased to 3.44 W in stage III. The slope efficiency in three stages was calculated to be 20%, 23% and 16%. The conversion efficiency in stage I and II was basically between 15% to 18% but it dropped to about 12% in stage III. A very strange phenomenon was that within pump power range of 30 W to 35 W, the 3.1 μm idler power in stage I was about 1.5 W higher than that in stage III. This difference was surely not caused by measurement error, external environment change or thermally induced optical bistability illustrated in Ref. [32]. This phenomenon was temporarily unexplained and needs further research. Figure 4(c) indicates that the 3.5 μm idler power linearly increased from 4.8 mW to 0.1 W in stage II and then to 0.5 W in stage III. The pump-to-idler slope efficiency in two stages

was calculated to be 1.54% and 7.6% separately. The conversion efficiency was around 1.5% in stage II and continuously increased to 3.5% at 14.43 W pump power in stage III. Both slope and conversion efficiency of the 1111 nm pump beam in stage II and III was much lower than that of the 1060 nm pump beam. It was analyzed that in stage II, the DFG process in which the 1111 nm pump beam was involved didn't satisfy phase-matching conditions and resulted in low parametric gain and efficiency. With increase of 1111 nm pump power in stage III, the DFG process gradually disappeared and phase-matched parametric oscillation built by 1111 nm pump beam arose, resulting in increasing conversion efficiency and higher slope efficiency. However, it was obvious that the 1111 nm pump power was near the OPO threshold or a little higher, also leading to low idler power and efficiency.

4. Conclusion

In summary, we demonstrated frequency down-conversion of DW Raman fiber laser and achieved DW mid-infrared output in a PPLN-based singly resonant OPO. The DW pump source was achieved based on SRS effect and located at 1060 nm and 1111 nm. With enhancement of SRS effect, the total, 1060 nm and 1111 nm pump power went through three stages. The DW idler beam was obtained in the latter two stages. The 1060 nm pump beam built independent parametric oscillation in all three stages and generated 1626 nm signal beam as well as 3056 nm idler beam. Different from the 1060 nm pump beam, the 1111 nm pump beam generated 3503 nm idler beam in stage II based on phase-mismatched DFG which occurred between 1111 nm and 1626 nm beams. With power increase in stage III, the 1111 nm pump beam built its own parametric oscillation, resulting in generation of new signal and idler beams fixed at 1621 nm and 3530 nm. The DW idler power ranged from 3.94 W to 7.78 W in stage II and III, in which the 3.1 μm and 3.5 μm idler power fluctuated with their corresponding pump power. The frequency down-conversion characteristics of 1060 nm and 1111 nm pump beams were also analyzed separately. An interesting phenomenon was found that under the same 1060 nm pump power, large difference existed in the 3.1 μm idler power with and without appearance of 1111 nm Raman laser, and it had no immediate explanation. However, the experiment results exhibited a limitation that was large power difference between two pump beams and between two idler beams. It can be solved in the further research by increasing length of passive fiber and 1060 nm pump power. This is, to the best of our knowledge, the first report on a DW mid-infrared OPO pumped by a DW Raman fiber laser. It was also the first time to combine fiber nonlinear effect and crystal nonlinear effect for mid-infrared generation. Its structure was very simple and easy to construct compared with other methods. The obtained 3.1 μm and 3.5 μm mid-infrared radiation are of great importance in some applications such as medical and biological diagnose, cascade pumping, trace gas sensing. The experiment results also revealed great potential in multi-wavelength mid-infrared generation with large wavelength gap using higher order SRS effect. It can be expected that these techniques will lead to a feasible scenario in many applications.

Acknowledgment

References

[1] T. Taniuchi, J. Shikata, and H. Ito, "Tunable terahertz-wave generation in DAST crystal with dual-wavelength KTP optical parametric oscillator," *Electron. Lett.*, vol. 36, no. 16, pp. 1414–1416, 2000.
[2] M. Wirth *et al.*, "The airborne multi-wavelength water vapor differential absorption lidar WALES: system design and performance," *Appl. Phys. B*, vol. 96, no. 1, pp. 201–213, 2009.
[3] J. Spigulis *et al.*, "Simultaneous recording of skin blood pulsations at different vascular depths by multiwavelength photoplethysmography," *Appl. Opt.*, vol. 46, no. 10, pp. 1754–1759, 2007.

[4] Y. Jia, K. Hanka, and K. T. Zawilski, P. G. Schunemann, K. Buse, and I. Breunig , "Continuous-wave whispering-gallery optical parametric oscillator based on CdSiP$_2$," *Opt. Exp.*, vol. 26, no. 8, pp. 10833–10841, 2018.

[5] X. Meng *et al.*, "Watt-level widely tunable femtosecond mid-infrared KTiOAsO$_4$ optical parametric oscillator pumped by a 1.03 μm Yb:KGW laser," *Opt. Lett.*, vol. 43, no. 4, pp. 943–946, 2018.

[6] B. Cole *et al.*, "Compact and efficiency mid-IR OPO sources pumped by a passive Q-switched Tm:YAP laser," *Opt. Lett.*, vol. 43, no. 5, pp. 1099–1102, 2018.

[7] M. Schellhorn, G. Spindler, and Marc Eichhorn, "Mid-infrared ZGP OPO with divergence compensation and high beam quality," *Opt. Exp.*, vol. 26, no. 2, pp. 1402–1410, 2018.

[8] L. Pomeranz *et al.*, "Efficient, 2–5 μm tunable CdSiP$_2$ optical parametric oscillator pumped by a laser source at 1.57 μm," *Opt. Lett.*, vol. 43, no. 1, pp. 130–133, 2018.

[9] D. J. Richardson, J. Nilsson, and W. A. Clarkson, "High power fiber lasers: Current status and future perspectives," *J. Opt. Soc. Amer. B*, vol. 27, no. 11, pp. 63–92, 2010.

[10] M. N. Zervas and C. A. Codemard, "High power fiber lasers: A review," *IEEE J. Sel. Topics Quantum Electron.*, vol. 20, no. 5, Sep.–Oct. 2014, Art. no. 0904123.

[11] Y. Jin *et al.*, "Broadly, independent-tunable, dual-wavelength mid-infrared ultrafast optical parametric oscillator," *Opt. Exp.*, vol. 23, no. 16, pp. 20418–20427, 2015.

[12] V. Ramaiah-Badarla, S. Chaitanya Kumar, and M. Ebrahim-Zadeh, "Fiber-laser-pumped, dual-wavelength, picosecond optical parametric oscillator," *Opt. Lett.*, vol. 39, no. 9, pp. 2739–2742, 2014.

[13] P. Jiang *et al.*, "A fiber laser pumped dual-wavelength mid-infrared optical parametric oscillator based on aperiodically poled magnesium oxide doped lithium niobate," *Laser Phys. Lett.*, vol. 10, 2013, Art. no. 115405.

[14] S. Cai *et al.*, "Compact tunable dual-wavelength mid-infrared optical parametric oscillator pumped by high power gain-switched fiber laser," *Laser Phys. Lett.*, vol. 12, 2015, Art. no. 075401.

[15] P. Wang, X. Cheng, X. Li, and X. Xu, "Tunable dual-wavelength, continuous-wave, mid-infrared generation using intracavity difference frequency mixing in PPLN-based optical parametric oscillator," *IEEE J. Sel. Topics Quantum Electron.*, vol. 24, no. 5, Sep.–Oct. 2018, Art. no. 0902807.

[16] R. G. Smith, "Optical power handling capacity of low loss optical fibers as determined by stimulated Raman and Brillouin scattering," *Appl. Opt.*, vol. 11, no. 11, pp. 2489–2494, 1972.

[17] F. Benabid *et al.*, "Stimulated Raman scattering in hydrogen-filled hollow-core photonics crystal fiber," *Science*, vol. 298, pp. 399–402, 2002.

[18] H. Kidorf, K. Rottwitt, M. Nissov, M. Ma, and E. Rabarijaona *et al.*, "Pump interactions in a 100-nm bandwidth Raman amplifier," *IEEE Photon. Technol. Lett.*, vol. 11, no. 5, pp. 530–532, May 1999.

[19] K. J. Blow and D. Wood, "Theoretical description of transient stimulated Raman scattering in optical fibers," *IEEE J. Quantum Electron.*, vol. 25, no. 12, pp. 2665–2673, Dec. 1989.

[20] D. I. Chang *et al.*, "Dual-wavelength cascade Raman fiber laser," *Electron. Lett.*, vol. 36, no. 16, pp. 1359–1358, 2001.

[21] A. M. R. Pinto *et al.*, "Interrogation of a suspended-core Fabry–Perot temperature sensor through a dual wavelength Raman fiber laser," *J. Lightw. Technol.*, vol. 28, no. 11, pp. 3149–3155, Nov. 2010.

[22] M. Lopez-Amo, M. Fernandez-Vallejo, and D. Leandro, "Bidirectional dual-wavelength Raman fiber ring laser," *IEEE Photon. Technol. Lett.*, vol. 23, no. 7, pp. 399–401, Apr. 2011.

[23] Q. Huang *et al.*, "Dual-wavelength single-mode optical fiber Raman laser," *Key Eng. Mater.*, vol. 532, pp. 367–372, 2013.

[24] S. Georgescu and O. Toma, "Er:YAG three-micron laser: Performances and limits," *IEEE J. Sel. Topics Quantum Electron.*, vol. 11, no. 3, pp. 682–689, May–Jun. 2005.

[25] L. Wang *et al.*, "Room temperature continuous-wave laser performance of LD pumped Er:Lu$_2$O$_3$ and Er:Y$_2$O$_3$ ceramic at 2.7 μm," *Opt. Exp.*, vol. 22, no. 16, pp. 19495–19503, 2014.

[26] J. Tafoya *et al.*, "Efficient and compact high-power mid-IR ($\sim$3 μm) lasers for surgical applications," in *Proc. Soc. Photo-Opt. Instrum. Eng.*, vol. 5312, 2004, pp. 218–222.

[27] K. L. Vodopyanov, I. Makasyuk, and P. G. Schunemann, "Grating tunable 4–14 μm GaAs optical parametric oscillator pumped at 3 μm," *Opt. Exp.*, vol. 22, no. 4, pp. 4131–4136, 2014.

[28] M. O. Fischer *et al.*, "DFB laser for sensing applications in the 3.0–3.5 μm wavelength range," in *Proc. Soc. Photo-Opt. Instrum. Eng.*, vol. 7945, 2011, pp. 79450E-1–79450E-13.

[29] H. Többen, "Room temperature CW fiber laser at 3.5 μm in Er^{3+}-doped ZBLAN glass," *Electron. Lett.*, vol. 28, no. 14, pp. 1361–1362, 1992.

[30] D. G. Lancaster *et al.*, "Real-time measurements of trace gases using a compact difference-frequency-based sensor operating at 3.5 μm," *Appl. Phys. B*, vol. 67, pp. 339–345, 1998.

[31] Y. Shang *et al.*, "Ultra-stable high-power mid-infrared optical parametric oscillator pumped by a superfluorescent fiber source," *Opt. Exp.*, vol. 24, no. 19, pp. 21684–21692, 2016.

[32] S. T. Lin *et al.*, "Observation of thermal-induced optical guiding and bistability in a mid-IR continuouswave, singly resonant optical parametric oscillator," *Opt. Lett.*, vol. 33, no. 20, pp. 2338–2340, 2008.